

**Clinical study of noninvasive *in vivo*
melanoma and nonmelanoma skin
cancers using multimodal spectral
diagnosis**

Liang Lim
Brandon Nichols
Michael R. Migden
Narasimhan Rajaram
Jason S. Reichenberg
Mia K. Markey
Merrick I. Ross
James W. Tunnell

Clinical study of noninvasive *in vivo* melanoma and nonmelanoma skin cancers using multimodal spectral diagnosis

Liang Lim,^a Brandon Nichols,^{a,†} Michael R. Migden,^b Narasimhan Rajaram,^{a,†} Jason S. Reichenberg,^c Mia K. Markey,^a Merrick I. Ross,^d and James W. Tunnell^{a,*}

^aUniversity of Texas at Austin, Department of Biomedical Engineering, 107 W. Dean Keeton Street C0800, Austin, Texas 78712, United States

^bUniversity of Texas MD Anderson Cancer Center, Department of Dermatology, 6655 Travis Street Suite 650, Houston, Texas 77030, United States

^cUniversity of Texas Southwestern-Austin, Department of Dermatology, 601 E 15th Street, Austin, Texas 78701, United States

^dUniversity of Texas MD Anderson Cancer Center, Surgical Oncology, 1400 Pressler Unit #1484, Houston, Texas 77030, United States

Abstract. The goal of this study was to determine the diagnostic capability of a multimodal spectral diagnosis (SD) for *in vivo* noninvasive disease diagnosis of melanoma and nonmelanoma skin cancers. We acquired reflectance, fluorescence, and Raman spectra from 137 lesions in 76 patients using custom-built optical fiber-based clinical systems. Biopsies of lesions were classified using standard histopathology as malignant melanoma (MM), nonmelanoma pigmented lesion (PL), basal cell carcinoma (BCC), actinic keratosis (AK), and squamous cell carcinoma (SCC). Spectral data were analyzed using principal component analysis. Using multiple diagnostically relevant principal components, we built leave-one-out logistic regression classifiers. Classification results were compared with histopathology of the lesion. Sensitivity/specificity for classifying MM versus PL (12 versus 17 lesions) was 100%/100%, for SCC and BCC versus AK (57 versus 14 lesions) was 95%/71%, and for AK and SCC and BCC versus normal skin (71 versus 71 lesions) was 90%/85%. The best classification for nonmelanoma skin cancers required multiple modalities; however, the best melanoma classification occurred with Raman spectroscopy alone. The high diagnostic accuracy for classifying both melanoma and nonmelanoma skin cancer lesions demonstrates the potential for SD as a clinical diagnostic device. © 2014 Society of Photo-Optical Instrumentation Engineers (SPIE) [DOI: 10.1117/1.JBO.19.11.117003]

Keywords: skin cancer; melanoma; *in vivo*; diagnosis; spectroscopy; Raman.

Paper 140323RR received May 21, 2014; revised manuscript received Sep. 21, 2014; accepted for publication Oct. 2, 2014; published online Nov. 6, 2014.

1 Introduction

Skin cancer is the most common cancer in the United States with an annual estimate of 3.5 million nonmelanoma skin cancer (NMSC) cases¹ and 70,000 melanoma cases.² NMSC is uncommonly fatal, but it can be locally destructive, spread to surrounding tissues, and give rise to complications. On the other hand, melanoma is the leading cause of death related to skin disease. Five-year relative survival rates of localized, regional, and distant melanomas are 98%, 61%, and 15%, respectively.³

Early diagnosis and treatment are currently the recommended management strategy for skin cancer; however, the current “gold standard” for diagnosis is invasive, costly, and time consuming. A diagnostic procedure consists of a clinical examination of the suspicious lesion, followed by biopsy and histopathology, with an additional turnaround time of approximately 1 week. When compared with histopathology, general practitioners’ diagnostic accuracy was reported to be between 24% and 44%, while dermatologists’ diagnostic accuracy was 77%.^{4,5} The common stance to err on the side of caution has led to performing an increased number of biopsies, where histopathology may be found to be negative for tumors. This

increases both the patient’s and health care financial burdens, with associated patient discomfort undergoing these additional surgical procedures. A more recent study reported a discordance rate of 14% among pathologists for melanoma diagnosis,⁶ highlighting the difficulty of accurately diagnosing melanoma even among experts. All these factors highlight the need for an objective, noninvasive, and faster method to aid a physician in diagnosing cancerous lesions, increasing clinical diagnostic accuracy while reducing unnecessary biopsies.

Optical spectroscopy offers a noninvasive alternative to measure tissue pathology. The interaction of light with tissue can provide insight into a tissue’s morphology and biochemical state. Weak and harmless light is delivered to sample the tissue under investigation. Analyzing the reemitted light provides structural and biochemical compositions such as specific protein content,^{7,8} nuclear morphology,^{9–11} oxygenation,¹² and hemoglobin concentration.¹³ As these parameters change with disease progression, optical spectroscopy provides an alternative to detect disease progression in an objective and noninvasive way. Cancer detection using optical spectroscopy has been reported for a variety of tissues such as bladder,^{14,15} breast,^{16,17} oral cavity,¹⁸ cervix,¹⁹ coronary arteries,^{20,21} Barrett’s esophagus,²² and skin.^{23,24}

Several commercial efforts have developed optical-based products that perform noninvasive melanoma skin cancer

*Address all correspondence to: James W. Tunnell, E-mail: jtunnell@mail.utexas.edu

[†]Brandon Nichols and Narasimhan Rajaram graduated from University of Texas at Austin and are currently at Duke University.

(MSC) diagnosis. These include MoleMax (Derma Medical Systems, Vienna, Austria), MelaFind (MELA Sciences, Inc., Irvington, New York), MoleMate (Biocompatibles, Surrey, United Kingdom), and SolarScan (Polartech Ltd, Sydney, Australia).²⁵ While studies with these devices have reported good diagnostic performance for MSC diagnosis,^{26–28} all of these devices are targeted only for MSC diagnosis. Clinical adoption of such devices will likely require a single device for characterizing both melanoma and NMSC.

Because of the strong need for a single device for the diagnosis of both melanoma and NMSC, several research efforts have focused on developing noninvasive optical spectroscopy techniques for combined diagnosis of malignant melanoma (MM) and NMSC. Zhao et al.²⁹ have developed an *in vivo* Raman spectroscopy (RS) technique with clinical verification of sensitivities and specificities of approximately 90% and 70%, respectively. Garcia-Urbe et al.³⁰ have used oblique incidence diffuse reflectance spectroscopy (DRS) to diagnose melanoma and NMSC with sensitivities and specificities of approximately 90%. These research efforts show great promise for optical spectroscopy's sensitivity to skin pathology; however, a successful clinical diagnostic device will require extreme accuracy. Because of melanoma's high mortality rate, high sensitivity will be required to avoid missing potential deadly lesions. At the same time, high specificity is needed in order to realize the benefits of such a device, to decrease the over-biopsy rate, and to reduce the costs and morbidity.

In an effort to increase the diagnostic accuracy, we propose a device based on multiple spectroscopic modalities. This approach takes advantage of the sensitivity of various spectral modalities to different tissue pathologies (e.g., light scattering is sensitive to cellular architecture while RS is sensitive to specific biomolecular bonds). Specifically, we combined three fiber-optic-based optical spectroscopy modalities: diffuse optical spectroscopy (DOS), laser-induced fluorescence spectroscopy (LIFS), and Raman spectroscopy (RS). DOS uses diffusely scattered light to determine tissue scattering and absorption,³¹ providing the tissue's microarchitecture, hemoglobin and melanin contents, and oxygen saturation. LIFS is sensitive to endogenous fluorophores⁷ such as metabolic coenzymes nicotinamide adenine dinucleotide (NADH) and flavin adenine dinucleotide, providing insight into cellular metabolism. In addition, LIFS measures structural protein status such as collagen and elastin,⁷

key indicators of a tumor's morphology and invasiveness.³² RS is sensitive to specific molecular vibrational energy levels, which are very common in biological tissue and skin. For example, the amide I bond is common in structural proteins such as collagen. Other Raman active molecules have allowed for the identification of specific tissue constituents such as lipids, water, cell nuclei, cell cytoplasm, and others.³³ As each optical spectroscopy technique is sensitive to specific and complementary interactions between light and tissue, a combination of modalities provides a more comprehensive picture of the tissue's biochemical and morphologic states. Previously, we reported that a combination of DOS and LIFS provides better NMSC diagnosis³⁴ than one technique alone. Volynskaya et al.¹⁷ reported that adding intrinsic fluorescence spectroscopy to DRS improves the diagnostic accuracy between subcategories of benign breast lesions by 12%.¹⁷

In this study, we describe the use of multimodal (RS, DOS, and LIFS) spectral diagnosis (SD) for noninvasive *in vivo* diagnosis of both melanoma and NMSC. SD's fast acquisition time (~5 s) is practical for *in vivo* measurements in a clinical setting. This study suggests that the multimodal SD has high diagnostic performance for *in vivo* melanoma (Se = 100%; Sp = 100%) and NMSC diagnosis (Se = 90% to 95%; Sp = 71% to 85%), and the multimodal nature of the technique contributes to this. Although RS contributes most highly to the diagnosis of melanoma, a combination of all techniques is required for good NMSC diagnosis. Our results demonstrate SD's potential as an *in vivo* melanoma and NMSC diagnostic tool that can help reduce unnecessary biopsies.

2 Materials and Methods

2.1 Spectral Diagnosis Clinical Instrument

Figure 1 shows the SD system in a clinical setting, with the system's schematic. The Raman instrument and fiber optic probe have previously been described in detail.^{35,36} The excitation source is an 830-nm diode laser (Lynx, Sacher Lasertechnik, Marburg, Germany). Excitation light is passed through a laser cleanup filter (Edmund Optics, Barrington, New Jersey) and coupled into a delivery fiber (NA = 0.22, 200- μ m core diameter). A simple sapphire ball lens at the distal tip of the probe improves light collection. Custom-in-line filters were placed between the fibers and ball lens to optimize light delivery

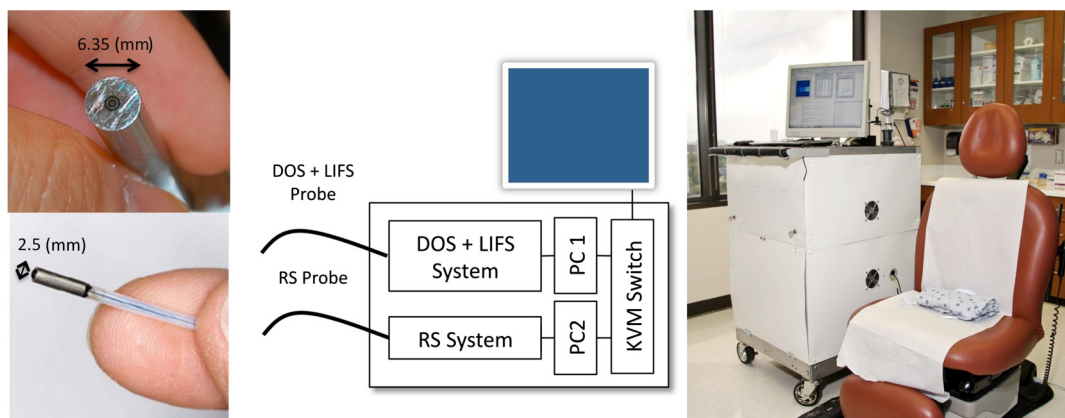


Fig. 1 Spectral diagnosis (SD) system in a clinical setting. It consists of two independent systems, each with a customized fiber optic probe. Details of the system are available in Sec. 2.

(short pass filter) and collection (long pass filter). Light collected at the distal tip of the probe then travel through the 15 collection fibers (NA = 0.27, 200- μm core diameter), which are linearly arranged at the proximal tip through a slit (200 μm) into a spectrograph (Kaiser Optical Systems HoloSpec f/1.8i, Ann Arbor, Michigan), and the spectrum is finally imaged onto a camera (Kodak KAF-1001E CCD, Finger Lakes Instrumentation, Lima, New York). Integration time is approximately 3 s. The collected spectra range is approximately 835 to 975 nm, corresponding to 84 to 1796 cm^{-1} Raman wavenumber shift relative to excitation source of 830 nm.

The combined DOS and LIFS system has been described in detail previously.³⁷ The excitation source for DOS is a pulsed xenon flash lamp (Hamamatsu Photonics, Bridgewater, New Jersey), and the excitation source for LIFS is a 337-nm pulsed nitrogen laser (Stanford Research Systems, Mountain View, California). Excitation sources are coupled to the center fiber of a 6-around-1 optical fiber probe (NA = 0.22, 200- μm core diameter, 200- μm source-detector separation, Fibertech Optica, Ontario, Canada) through a fiber optic switch (FSM-13, Piezosystems Jena, Jena, Germany). Light collected at the distal tip of the probe travels through the collection fibers, which are linearly arranged at the proximal tip into a spectrograph (SP-150, Princeton Instruments, Trenton, New Jersey), and the spectra are imaged onto a thermo-electrically cooled CCD (Coolsnap, Princeton Instruments). Total integration time for a complete measurement (DOS, LIFS, and background) is less than 0.5 s. The collected spectra range is approximately 330 to 690 nm.

2.2 Patient Recruitment

This study was approved by the Institutional Review Board at The University of Texas at Austin and The University of Texas MD Anderson Cancer Center (trial registration ID: NCT 00476905). Informed consents were acquired from all patients prior to the study. We acquired *in vivo* DOS, LIFS, and RS spectra from 137 lesions in 76 patients. Enrolled patients' age ranged from 22 to 93 years, with an average age of 62. Enrolled patients were predominantly male (male 71%, female 24%, NA 5%) and Caucasian (Caucasian 91%, Hispanic 1%, Asian/Pacific Islander 1%, NA 7%). NA (not available) accounts for missing entries from incomplete patient surveys.

Corresponding biopsies were acquired from each lesion site and classified using standard histopathology by a board certified pathologist as MM (12 lesions), nonmelanoma pigmented lesion (PL, 17 lesions), basal cell carcinoma (BCC, 19 lesions), actinic keratosis (AK, 14 lesions), and squamous cell carcinoma (SCC, 38 lesions). Fourteen out of the 38 SCC lesions have features of both AK and SCC. Sixteen lesions (e.g., scar, seborrheic keratosis) did not fall under any of the previous groups. Twenty-one lesions were excluded from the analysis from bad data (4 lesions), incomplete data (13 lesions), and small lesions (4 lesions). Bad data consisted of measurements with saturated and high background signal. Incomplete data consisted of measurements without all three modality's measurements. These errors occurred when fibers in our DOS + LIFS probe broke, and on instances when the Raman system failed in its initialization process. We also excluded lesions smaller than 2 mm in diameter. Our DOS + LIFS probe sleeve is 6.35 mm in diameter, which posed a challenge in measuring lesions smaller than the probe diameter. This version of the instrument also required the room lights to be turned off to reduce ambient light influences

on the spectral data, making it more difficult to position probes on small lesions.

2.3 Acquisition Procedure

SD measurements were conducted prior to lesion biopsy. Each measurement consisted of spectral data from each modality (RS, DOS, and LIFS). Care was taken to position both probes in the same location. We acquired measurements from multiple spots on each lesion [average measurements (range) per corresponding lesion = 2.2 (2 to 4)] followed by measurements of nearby corresponding normal skin [average measurements (range) per corresponding normal skin = 2 (1 to 3)]. Although none of the normal skin measurements were verified by histopathology, we ensured that the normal skin measurements were acquired at an area close to the lesion and visually verified to be normal by an experienced dermatologist/physician assistant. A biopsy was performed on the lesion, and the histopathology results were recorded. Histopathology for the lesion was applied for all the measurements on that lesion. We developed a numbering system to keep the correct corresponding histopathology results with our measurements without compromising patients' privacy and information.

2.4 Data Processing and Calibration

All spectral data underwent background noise removal. DOS and LIFS data processing and calibration were processed as described by Rajaram et al.³⁷ Briefly, DOS data are intensity calibrated to a liquid phantom solution of polystyrene microspheres (1 μm , Polysciences, Warrington, Pennsylvania). LIFS data are intensity calibrated to a liquid phantom of Rhodamine (Rhodamine B, Sigma-Aldrich, St. Louis, Missouri) and spectrally calibrated to a NIST traceable tungsten calibration standard (LS-1-CAL, Ocean Optics, Dunedin, Florida). DOS and LIFS spectra were wavelength calibrated using a mercury argon calibration source (HG-1, Ocean Optics).

RS data underwent cosmic ray removal and fluorescence removal using a fifth-order modified-polynomial fitting routine.³⁸ Raman spectral data were wavenumber calibrated with daily measurements of acetaminophen. For our analysis, data under 800 cm^{-1} were excluded because of strong sapphire peaks around 400 and 750 cm^{-1} and fiber background signal around 800 cm^{-1} .

2.5 Standardization of Diffuse Optical Spectroscopy and Laser-Induced Fluorescence Spectroscopy

Visual observation of multiple individuals' skin will show that the spectral variance between individuals' normal skin is high. Even among the same individual, variance of normal skin from different anatomical sites is high. Meaningful comparison between different anatomical sites and individuals can only be achieved after standardization of all measurements from all patients to a baseline or reference point. We have previously described a standardization technique for both DOS and LIFS spectral data.³⁴ LIFS spectral data were standardized using the following equations:

$$N_i(\lambda) = \frac{N_i(\lambda)}{\max[N_1(\lambda)]} \times N_{\text{mean}}, \quad (1)$$

$$L_i(\lambda) = \frac{L_i(\lambda)}{\max[N_1(\lambda)]} \times N_{\text{mean}}, \quad (2)$$

where $N_i(\lambda)$ and $L_i(\lambda)$ represent the wavelength-dependent fluorescence spectra from normal skin and lesion, respectively. $N_1(\lambda)$ is the first normal skin spectra measurement for each patient's lesion, and N_{mean} is the mean LIFS value for all normal skin sites collected in this study. The basic premise behind this standardization technique is to standardize every patient's normal skin measurement and to adjust the corresponding lesion measurement by the same scale.

In this study, we modified this standardization technique to better suit DOS data using the following standardization equations:

$$N_i(\lambda) = \frac{N_i(\lambda)}{\max[N_1(630 - 690 \text{ nm})]} \times N_{\text{mean}}(630 - 690 \text{ nm}), \quad (3)$$

$$L_i(\lambda) = \frac{L_i(\lambda)}{\max[N_1(630 - 690 \text{ nm})]} \times N_{\text{mean}}(630 - 690 \text{ nm}). \quad (4)$$

Light scattering is the dominant contributor to DOS spectra in the 630- to 690-nm wavelength region, with less influence by melanin and hemoglobin absorptions. By restricting the DOS standardization wavelength range to 630 to 690 nm, DOS standardization is less unpredictable and more anchored around scattering. This standardization emphasizes tissue scattering, which we have reported to be a strong diagnostic parameter for NMSC.³⁴ Further details on how this standardization procedure impacts diagnosis are available in Appendix A1.

2.6 Statistical Analysis and Classification

Processed spectral data were then grouped to their classification datasets (MM versus PL, SCCBCC versus AK, and AKSCCBCC versus normal). Principal component analysis (PCA) was performed on each classification dataset for each modality. PCA is adept at dimensional reduction of spectral data. Using multiple highest varying principal components (PC), we built leave-one-out logistic regression classifiers for melanoma (MM versus PL) and nonmelanoma (SCCBCC versus AK and AKSCCBCC versus normal) skin cancers. Leave-one-out cross-validation is preferred when sample size is small and logistic regression is simple to implement.

We limited the PCs used for classification to those that accounted for the highest variance from each modality. The most significant 10, 2, and 2 PCs accounted for the majority (95%) of the variance in each modality (RS, DOS, and LIFS, respectively). The higher number of significant PCs in Raman as compared with DOS and LIFS is expected as DOS and LIFS spectral features are not as varied compared with Raman, which has multiple well-defined and narrow peaks. We surveyed every possible combination of the most significant PCs and identified the combination of PCs for the optimum sensitivity and specificity. We limited the total number of PCs used in the classification to seven, because in most cases, the diagnostic performance stopped improving significantly beyond five PCs. Classification results were compared with histopathology of the lesion. In this article, PC of a particular modality is

labeled by the modalities' first letter and the PC's rank. For example, D2 refers to DOS PC 2 and R1 refers to RS PC 1.

We determined sensitivity and specificity using a conservative per lesion analysis approach, as mentioned in our previous study,³⁴ and demonstrated in this Appendix A3. Per lesion analysis classifies a lesion as positive, if any one of the lesion's measurements is classified as positive. Conversely, all of the lesion's measurements have to be classified as negative in order for the lesion to be considered as negative.

3 Results

3.1 Spectral Variations Between Pathologies by Modalities

Figures 2(a) and 3(a) show the mean Raman spectra of melanoma and NMSC pathologies, respectively. Prominent Raman bands are highlighted.^{39,40} Major contributors of Raman signal in skin are lipids and proteins. By visual inspection, we observed several spectral differences between pathologies. PL and MM showed decreased intensity of amide I spectral region, resulting in spectral flattening between 1500 and 1800 cm^{-1} and increased intensity in the 1310 to 1340 cm^{-1} lipid band. PL and MM showed peaks between 800 and 900 cm^{-1} that are absent from all other pathologies. MM and BCC showed lower intensity in the 1450- cm^{-1} region.

A major source of Raman signal in skin is from the protein collagen,⁸ which is abundant with amide linkages. Increased melanin and pigmentation in MM and PL explain the reduced collagen's Raman signals and spectral flattening in the amide I region, consistent with studies by other groups.^{41,42} Melanin has two broad Raman peaks in the 1380- and 1580- cm^{-1} wavenumber region, contributing to the flattening of Raman signal in these wavenumber regions.⁴³ The flatter amide I region in MM could be indicative of further degradation of collagen in MM with respect to PL. Spectral changes in amide I and amide III are also effective diagnostic parameters in NMSC, as they are prominent Raman features in PCs used in those classifications. Various diagnostic PCs have features located between 800 and 950 cm^{-1} that may represent contributions from amino acids such as tyrosine (830, 853 cm^{-1}) and proline (853, 920 cm^{-1}), and at 1300 and 1340 cm^{-1} that may represent contributions from lipids, mainly from ring breathing and C-C stretching, and DNA components such as adenine (1336 cm^{-1}). Tyrosine is a precursor of melanin, and tyrosine phosphatase genes (regulators of tyrosine phosphorylation) have been shown to be downregulated in melanoma.⁴⁴ Tyrosine phosphorylation has been shown to induce collapse of the doublet around 820 to 850 cm^{-1} , attenuation of the peak at 1205 cm^{-1} , and shift of the amide III band.⁴⁵

Figures 2(b) and 3(b) show the mean DOS spectra by pathology. DOS measurement is a function of optical scattering and absorption. The primary sources of scattering in skin include collagen, mitochondria, melanin, and cell nuclei. Hemoglobin and melanin are the primary sources of absorption in skin. Determined by visual inspection, the two most diagnostically significant PCs contribute to reflectance spectral intensity and spectral slope (D1 and D2, respectively). Although PCs do not directly indicate optical properties, Skala et al.⁴⁶ have demonstrated that the first DOS PC correlates strongly with reduced scattering coefficient. With our fiber optic geometry, scattering from dermal collagen dominates epidermal scattering from cells and nuclei. All pathologies have lower reflectance intensities

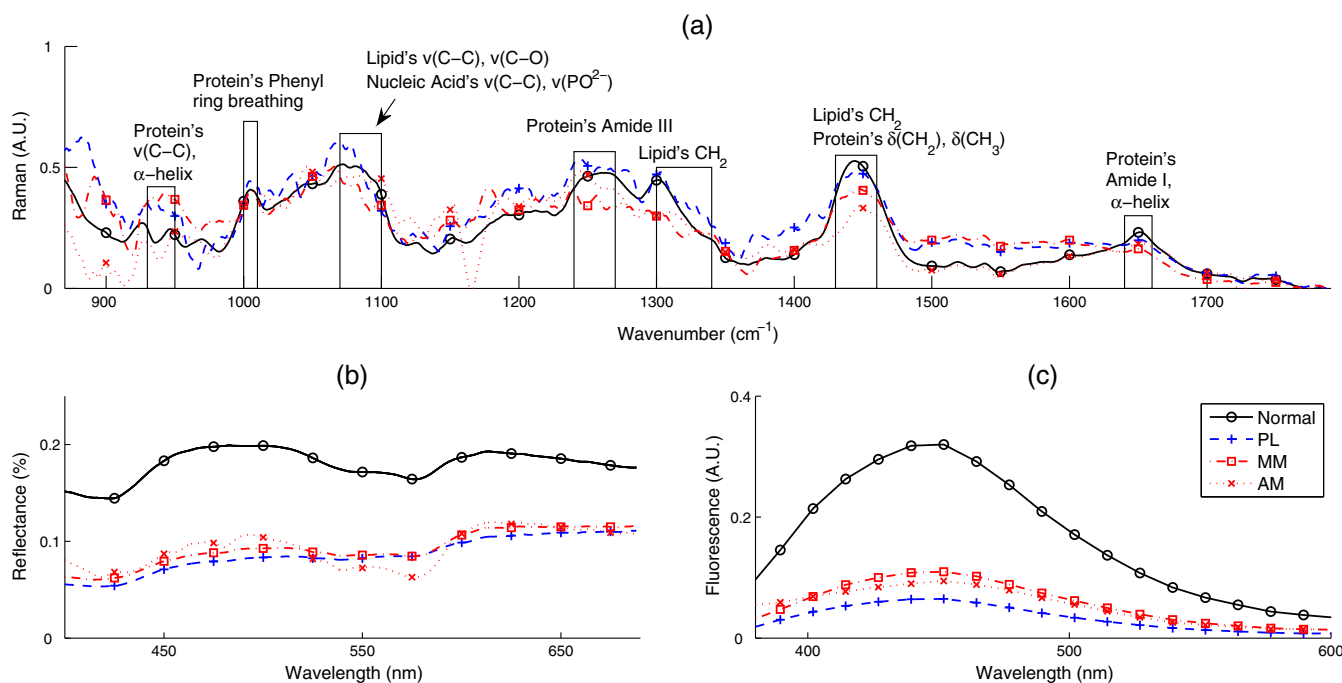


Fig. 2 Mean spectra of melanoma (MM) nonmelanoma pigmented lesions (PL), and normal skin. One of the melanoma lesions is an amelanotic melanoma (AM): (a) RS, (b) DOS, and (c) LIFS.

compared with normal skin. Melanoma and nonmelanoma pigmented lesions (MMPL) have lower overall intensity and slightly different DOS spectral slope, mostly because of more absorption from higher melanin content. In NMSC, decrease in reflectance intensity of lesions is most likely because of a decrease in scattering coefficient, which indicates the breakdown of collagen present in the dermis. Another possible explanation is that the thickening of epidermis from the progression of malignancy^{47,48} reduces the amount of collagen being sampled, and thus the overall scattering of the cancerous lesion is lower compared with normal skin. Other studies have observed lower scattering coefficient in neoplastic lesions.^{24,34,49} AK differed from SCC in spectral slope and absorption. SCC shows the higher reflectance intensity around 400 to 475 nm.

Figures 2(c) and 3(c) show the mean LIFS spectra by pathology. The main fluorophores from human skin using 337-nm excitation wavelength are collagen and NADH. Both AK and SCC fluorescence intensities are higher compared with normal skin, with AK's fluorescence peak slightly red-shifted compared with SCC's fluorescence peak. PL and MM have much lower fluorescence intensity compared with all the other pathologies.

Table 1 summarizes the sensitivity and specificity of all classifiers for all modalities using per lesion analysis and the corresponding PCs that provided the optimal diagnostic accuracy. Corresponding receiver operating characteristic curves are shown in Fig. 4.

3.2 Melanoma Skin Cancer and Pigmented Lesions

One of the primary spectral differences between MMPL and normal skin is the much lower DOS and LIFS. This is expected as we can visually observe that MMPL is darker compared with normal skin. Melanin's absorption overlaps with fluorescence emission from major fluorophores in skin, explaining the much lower fluorescence intensity from MMPL. This makes DOS and LIFS intensities as excellent parameters in diagnosing

MMPL from normal skin. Using just two PCs (D1 and R9 or L1 and R9), we can distinguish normal skin from MMPL with sensitivity/specificity of 100%/100%.

However, this makes DOS and LIFS intensities as poor diagnostic parameters in differentiating MM from PL. As MM and PL can be lightly pigmented or heavily pigmented, both MM and PL overlap in DOS and LIFS intensities. Nevertheless, five PCs from RS were able to distinguish MM from PL with sensitivity/specificity of 100%/100%. Diagnostic Raman PCs for MM versus PL correspond to Raman spectra in the amide I, 1300–1340 lipids, amide 3, CH₂ around 1450 cm⁻¹, and regions around 800 to 1000 cm⁻¹.

One amelanotic melanoma (AM) lesion was included in our melanoma dataset (plotted as the dotted-cross-line in Fig. 2). AM is a rare type of melanoma without the pigmentation that normally accompanies pigmented lesions (often mistaken as BCC), thus challenging to notice and diagnose visually. A couple of interesting observations can be made on this lesion's spectra. The AM's DOS and LIFS intensities were close to that of the MM's and PL's spectra. AM's Raman spectra also showed lower CH₂ (1450 cm⁻¹) and amide I (1650 cm⁻¹) vibrations, like MM and PL. The absence of melanin pigmentation is consistent with the lack of melanin peaks around 1380 and 1580 cm⁻¹, thus having a Raman profile more similar to normal skin at these wavenumber regions. The AM's Raman spectra in the 900 to 1300 cm⁻¹ are most similar to MM. In our case, the AM was still correctly classified as positive for melanoma.

3.3 Nonmelanoma Skin Cancer

In general, DOS and LIFS PCs were more prominent in the diagnosis of NMSC. One of the main spectral features of NMSC compared with normal skin is the lower DOS reflectance spectra intensity, as shown in Fig. 3(b). Decrease in reflectance intensity of lesions is most likely from a decrease in scattering coefficient, which indicates breakdown of collagen present in

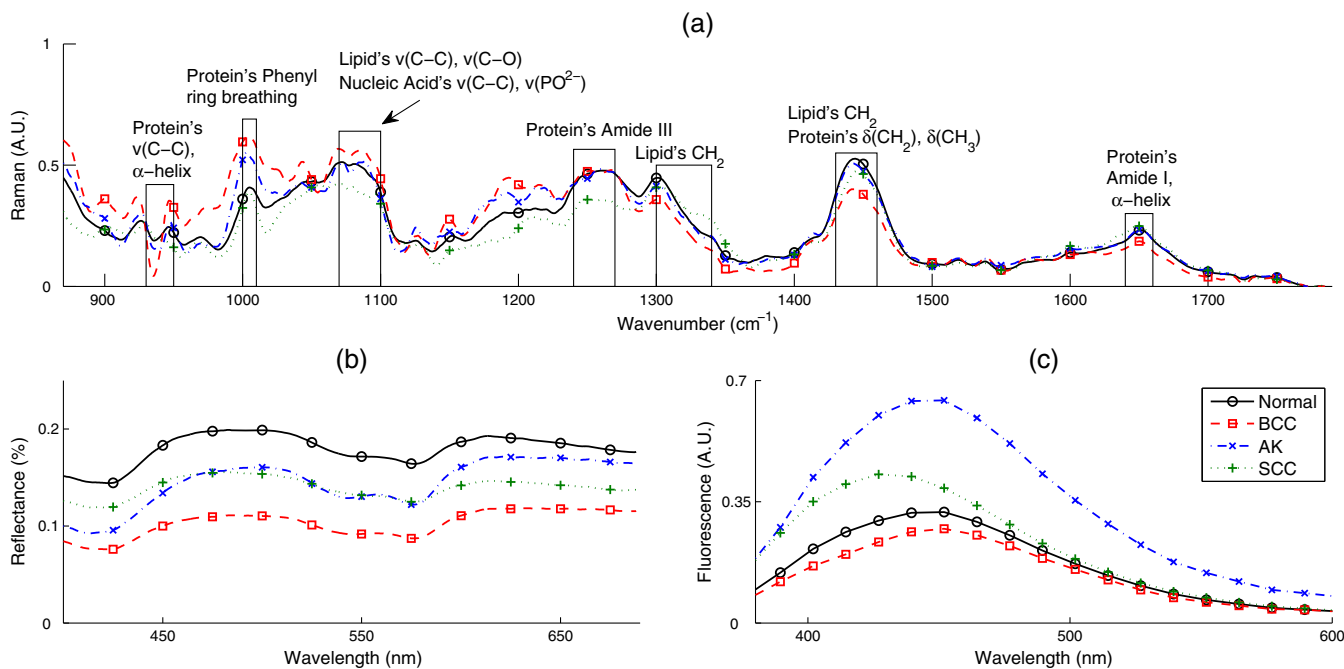


Fig. 3 Mean spectra by pathology for nonmelanoma skin cancer (NMSC; BCC, SCC, and AK) compared with normal skin: (a) RS, (b) DOS, and (c) LIFS.

Table 1 Sensitivity/specificity (%) summary table using per lesion analysis. Accuracy is the percentage of correct classifications [(true positive + true negative)/total lesions]. For instance, for SCCBCC versus AK, true positive = $0.95 \times 71 = 54$, true negative = $0.71 \times 14 = 10$, total lesions = 71, and accuracy = $(54 + 10)/71 = 90\%$. Best diagnostic performance with the least number of modalities and/or PCs are in bold.

Classifier	# Lesions	Sensitivity/Specificity (%)				Accuracy (%)
		RS	DOS	LIFS	Combined	
MM versus PL	12 versus 17	100/100 R3, R5, R8, R4, R9	17/59	67/18	100/100	100
MMPL versus norm.	29 versus 28	90/82	97/100	93/100	100/100 (D1, R9) or (L1, R9)	100
SCCBCC versus AK	57 versus 14	72/64	75/71	91/57	95/71 D2, L2, R9	$(54 + 10)/71 = 90$
AKSCCBCC versus norm.	71 versus 71	68/55	87/68	52/52	90/85 D1, D2, L1, L2, R7	$(64 + 60)/142 = 87$

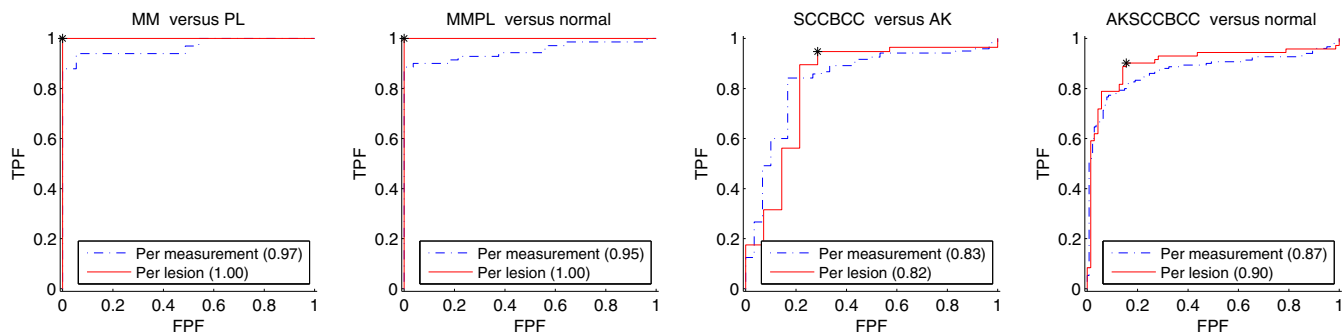


Fig. 4 Receiver operating characteristic curves for all classifiers, with corresponding area under the curve (AUC) shown in legend. The sensitivity and specificity for each classifier are marked. We use per lesion analysis, described in Sec. 2.

the dermis, or thickening of epidermis from the progression of malignancy,^{47,48} reducing the sampling of highly scattering collagen. Thus, the overall scattering of the cancerous lesion is lower compared with normal skin, consistent with reports in the literature.^{24,34,49} However, DOS spectral intensity might not be a reliable parameter in diagnosing SCC and BCC from AK, as their mean spectra overlap with a smaller distribution. LIFS on the other hand is not as straightforward. Mean LIFS spectra from diseased skin (AK, SCC, and BCC) are distributed all around the mean spectrum of normal skin.

A combination of PCs from all modalities is needed for effective NMSC diagnosis. Five PCs (D1, D2, L1, L2, and R7) resulted in the best classification of AKSCCBCC versus normal skin, providing sensitivity/specificity of 90%/85%. A more clinically relevant diagnosis is to differentiate SCC and BCC from AK. AK has been hypothesized to be a precursor of SCC.⁵⁰ Treatments for AK vary from external topical medication to surgery, while SCC and BCC are almost always removed surgically. A combination of three PCs (D2, L2, and R9) resulted in the best classification between SCCBCC (biopsy and surgical excision) versus AK (cryotherapy/topical cream treatment), providing sensitivity/specificity of 95%/71%. Also, as we expected, D1 (main contributor to spectral intensity) is not one of the diagnosis parameters for SCCBCC versus AK.

4 Discussion

4.1 Future Work

We envision that our classifiers could be applied in a clinical setting via a simple two-step process. For the first step, a physician will choose the MSC or NMSC classifier. For the second step, if MSC was chosen, the classifier will classify MM (positive, biopsy) from PL (negative, observation). The negative group will eventually need to include lesions such as pigmented BCC and SK, which are commonly suspected as melanoma. If NMSC was chosen, then the classifier will classify SCCBCC (positive, biopsy, and surgical excision) from AK (negative, cryotherapy/topical treatment). The outcome of the classifiers will diagnose the lesion and also indicate the lesion's treatment.

In this study, we applied a purely statistical approach (PCA) to analyze and classify the data. While PCA is a powerful technique, it does not elucidate the underlying physiological basis for the diagnosis. Physiological-based models can be used to determine the underlying chemical, physiological, and morphological statuses of tissues.^{21,33} For example, we have previously demonstrated a DOS model that can extract physiological parameters such as hemoglobin content, oxygen saturation, and tissue microarchitecture.^{34,51} Haka et al.³³ demonstrated an RS physiological model for determining lipid, nuclear, and protein content from breast tissues. However, an RS physiological model for skin currently does not exist. Such a model would allow similar physiological components to be extracted from measured skin RS data and potentially explain the underlying physiological basis for the diagnosis.

Our results also indicate that PCA may not be sensitive to important pathological changes. For instance, LIFS PCs were only used in diagnosis of AK and SCC and only performed well when combined with other modalities. Panjehpour et al.⁵² reported that LIFS alone was capable of good diagnostic performance of BCC and SCC from normal and benign lesions, suggesting that our simple PC analysis was not robust enough to detect pathological changes seen in that study. One important

note is that the PC approach does not allow for the correction of tissue fluorescence for distortions from tissue optical absorption and scattering. This correction has been noted to be an important factor in other organs,⁵³ and may further improve the diagnosis of this modality.

While this study used two separate systems to acquire three modalities, our lab has developed a multimodal system to acquire all three modalities using a single optical fiber probe and instrument.⁵⁴ This will reduce sampling site error and clinical acquisition time.

4.2 Conclusion

We implemented DOS, LIFS, and RS as a noninvasive *in vivo* diagnostic for melanoma and NMSC. We collected *in vivo* measurements of 137 lesions from 76 patients and built leave-one-out logistic regression classifiers using PCs from each modality. Our results demonstrate the ability of these modalities to quantitatively assess tissue biochemical, structural, and physiological parameters that can be used to determine tissue pathology with high accuracy. We compared the diagnostic capabilities between each spectroscopy modalities for both melanoma and NMSC. Individual modalities can achieve very good diagnostic results. PCs from RS were able to diagnose MM from PL with 100% accuracy. However, a combination of PCs from all modalities is needed to properly diagnose NMSC. As a whole, a combination of all three modalities is necessary for *in vivo* noninvasive diagnosis of both melanoma and NMSC.

In conclusion, these results show good diagnostic performance of noninvasive *in vivo* diagnosis of melanoma and NMSC using multiple optical spectroscopy modalities. An accurate, fast, and objective skin cancer diagnosis device has the potential to improve skin cancer diagnosis and to reduce unnecessary biopsies. This high diagnostic performance applicable to both melanoma and NMSC shows great promise as a clinical diagnostic tool.

Appendix: Miscellaneous Details on Materials and Methods

A1 Standardization of DOS and LIFS Data

The effect of DOS and LIFS standardization is shown in Fig. 5. Specific to our sample pool, note that the mean DOS and LIFS spectra of the normal skin from the PL group are significantly higher than the mean spectra of all normal skin measurements [Figs. 5(a) and 5(c)]. On the contrary, the mean DOS and LIFS spectra of normal skin from the MM group are lower than the mean spectra of all normal skin measurements. After standardization, DOS and LIFS spectra from normal skin are more tightly spaced together [Figs. 5(b) and 5(d)], whereas the corresponding MM and PL spectra are adjusted accordingly. MM and PL spectra are also more tightly spaced together.

The benefit of standardization is obvious when we compare sensitivity/specificity before and after standardization, as summarized in Table 2. The biggest benefit for both standardization techniques is in diagnosing MMPL from normal skin. Without any standardization, two DOS PCs or two LIFS PCs were able to classify MMPL from normal skin with sensitivity/specificity of 93%/89% and 83%/100%, respectively. After standardization, one DOS PC or one LIFS PC was better in classifying MMPL from normal skin with sensitivity/specificity of 97%/100% and 93%/100%, respectively. This is expected as

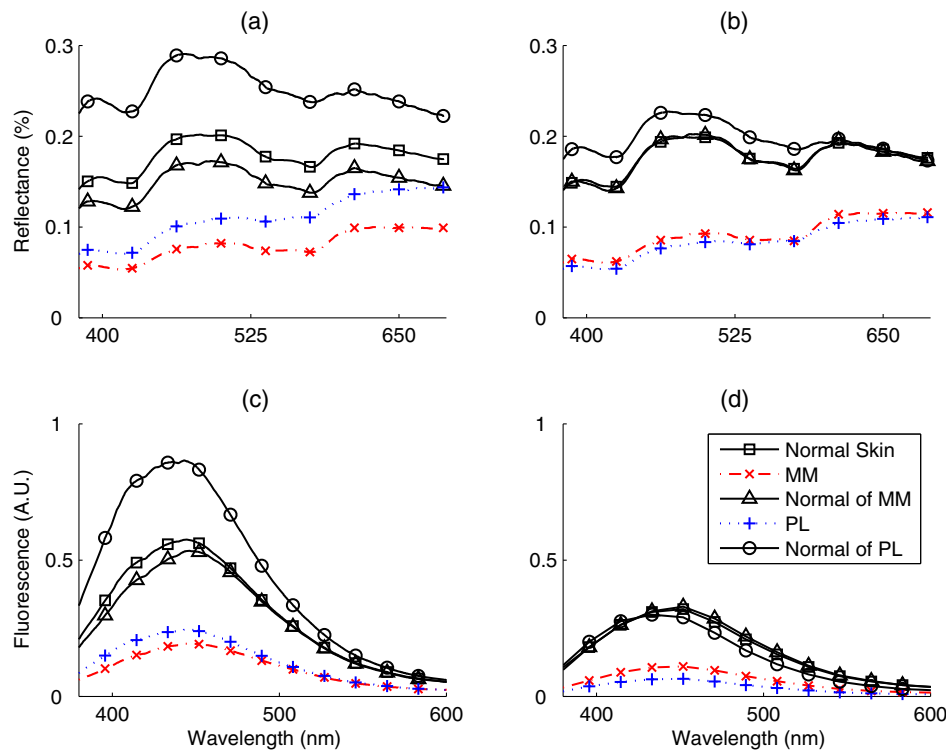


Fig. 5 Effect of standardization on DOS (a, b) and LIFS data (c, d): DOS prestandardization (a) and poststandardization (b), and LIFS prestandardization (c) and poststandardization (d).

standardization narrows the distribution of normal skin measurements, and as a result, narrows the distribution of MMPL measurements.

DOS's ability to classify MM from PL is reduced (from 92%/53% to 17%/59%). This might first appear to be disadvantageous, but it is likely more representative of the clinical setting. Spectral intensity, which is directly correlated with pigmentation of a lesion, is not a reliable diagnostic parameter for discriminating MM from PL. Both MM and PL can be light (e.g., amelanotic), or extremely dark, with every shade in between. The better sensitivity/specificity of unstandardized MM versus PL based on DOS spectral intensity and shape (D1 and D2) is only specific to this unstandardized sample pool, because most of the MM in this sample pool happened to have lower DOS spectral intensity. Overall, standardization is a key step in processing DOS and LIFS spectral data for malignancy

diagnosis. It removes the variances due to normal anatomy and enhances the variances due to disease.

A2 Standardization of Raman Spectroscopy

The importance of standardization on DOS and LIFS implied a similar need of standardization for RS data. Research groups have implemented various standardization techniques for measurements from skin. Several standardization techniques reported in the literature include: (1) scaling the area under the curve (AUC) to 1,⁵⁵ (2) zeroing the mean with unit variance,^{56,57} (3) standardizing to mean intensity,⁴¹ and (4) scaling to Raman peak intensity.^{42,58} Each has its merits, but a consensus has not been established regarding the proper standardization technique for Raman measurements of human skin tissue.

Our general standardization approach was to normalize to a prominent benchmark that was present in all measurements.

Table 2 Effect of standardization on DOS and LIFS sensitivity/specificity (%).

Standardization	# Lesions	DOS Sensitivity/Specificity (%)		LIFS Sensitivity/Specificity (%)	
		Pre	Post	Pre	Post
MM versus PL	12 versus 17	92/53 D1, D2	17/59 D1	66/6 L1, L2	67/18 L1, L2
MMPL versus normal	29 versus 28	93/89 D1, D2	97/100 D1	83/100 L1, L2	93/100 L1
SCCBCC versus AK	57 versus 14	70/57 D2	75/71 D2	60/57 L2	91/57 L2
AKSCCBCC versus normal	71 versus 71	82/70 D1, D2	87/68 D1, D2	54/51 L2	52/52 L2

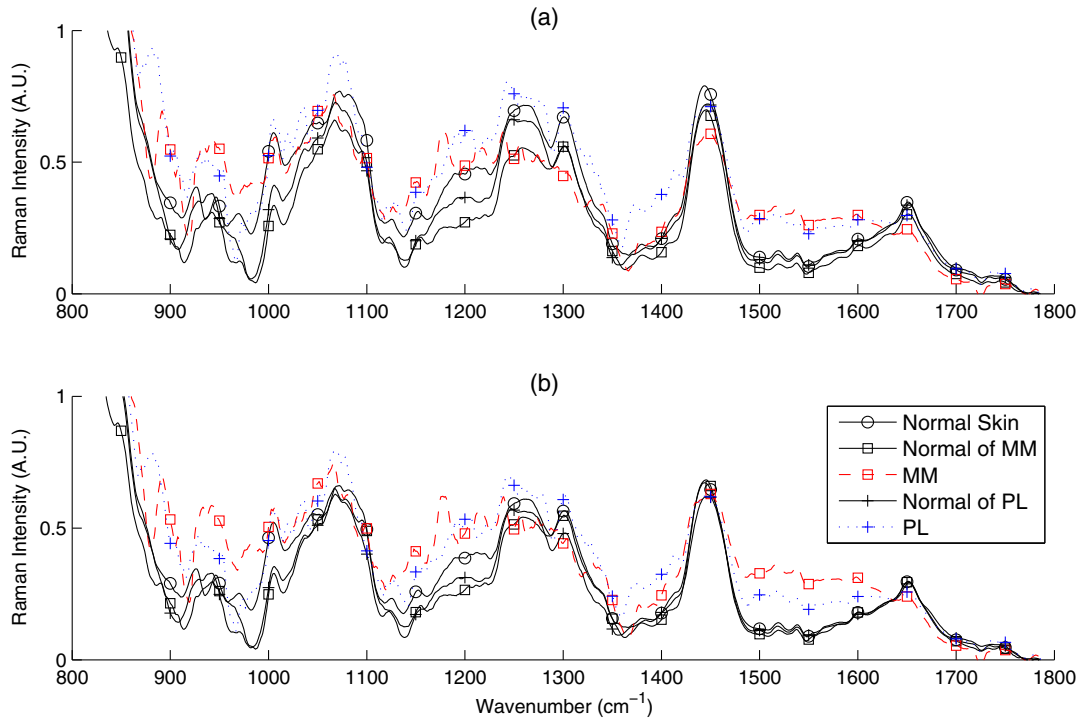


Fig. 6 RS standardization to AUC of amide I peak (1642 to 1660 cm^{-1}). (a) RS prestandardization and (b) RS poststandardization.

Specifically, we normalized to the AUC of the amide I Raman peak centered at 1650 cm^{-1} . For consistency with our DOS and LIFS, we standardized using the lesion's first normal measurement, as shown by the following equations:

$$N_i(\lambda) = \frac{N_i(\lambda)}{\text{AUC}[N_1(1642 - 1660)]}, \quad (5)$$

$$L_i(\lambda) = \frac{L_i(\lambda)}{\text{AUC}[N_1(1642 - 1660)]}. \quad (6)$$

Figure 6 illustrates the effect of standardization on the RS data, and Table 3 summarizes the sensitivity/specificity differences between standardized and unstandardized RS data. Mean Raman spectra of normal skin from each pathology group were closer (e.g., in the spectral regions of 1650 and 1450 cm^{-1}), resulting in less variance between PL and MM (i.e., mean spectra of PL and MM are closer around 1650, 1450, 1200 to 1300 cm^{-1}). Unfortunately, amide I is an important diagnostic peak, and thus, standardization to this peak

reduced its variance and the resulting effectiveness of this “standardized” RS diagnosis.

Because amide I exists in various physiological components in skin,^{21,59} standardizing RS data to it may not highlight tissue pathology appropriately. While DOS and LIFS standardizations were anchored around one or two physiological components, RS standardization to amide I was likely from multiple physiological components. RS is very different in spectral profile (i.e., many narrow peaks from various contributing physiological parameters). Thus, RS may require a more intricate standardization procedure. More study is needed to determine an appropriate standardization technique for RS. For this study, we reported results from both standardized and unstandardized RS data, and we use the unstandardized RS data in reporting our final diagnostic performance.

A3 Per Lesion Analysis

We determined sensitivity and specificity using a conservative per lesion analysis approach. Our acquisition procedure acquired multiple measurements from the same lesion, and the classification was performed on a per lesion basis. This is in

Table 3 Effect of standardization on RS sensitivity/specificity (%).

Classifier	# Lesions	Raman Unstandardized		Raman Standardized	
		RS Se./Sp. (%)	Combined Se./Sp. (%)	RS Se./Sp. (%)	Combined Se./Sp. (%)
MM versus PL	12 versus 17	100/100	100/100	92/88	92/88
MMPL versus normal	29 versus 28	90/82	100/100	76/89	100/100
SCCBCC versus AK	57 versus 14	72/64	95/71	81/50	91/79
AKSCCBCC versus normal	71 versus 71	68/55	90/85	80/52	92/79

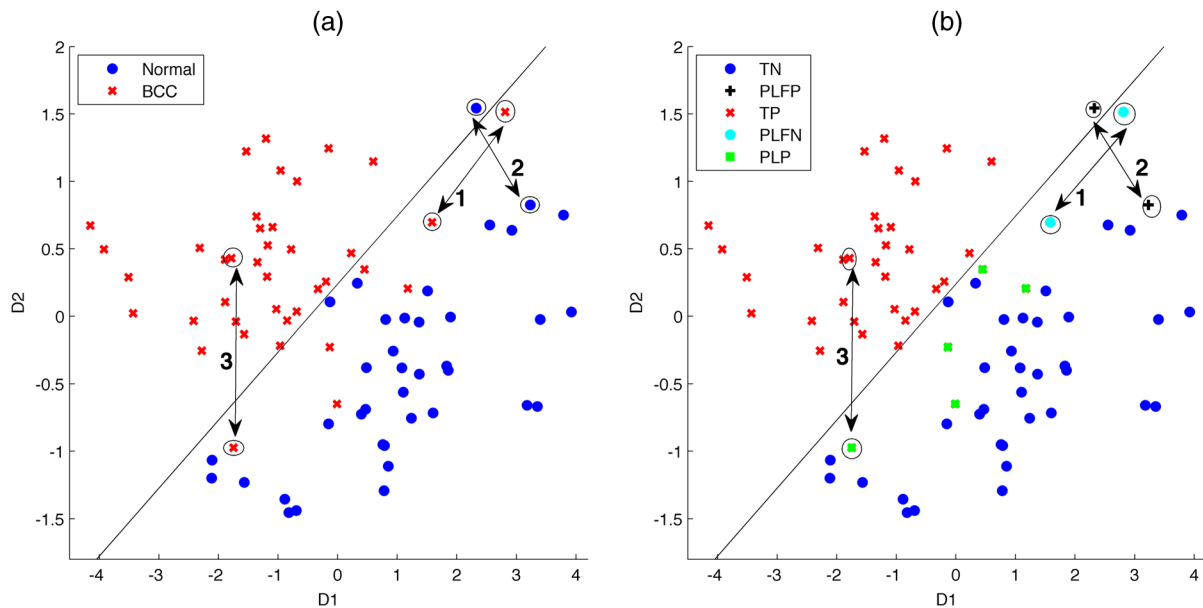


Fig. 7 PC scores (D1 and D2) for classifying BCC versus normal (N) using per measurement analysis (a) versus per lesion analysis (b). For better visualization, this plot zooms at the region around the decision line. Legends: TN = true negative (normal skin measurements on the negative side of the decision line), PLFP = per lesion false positive (normal skin measurements with at least one measurement on the positive side of the decision line), TP = true positive (BCC measurements on the positive side of the measurements), PLFN = per lesion false negative (all measurements from the same BCC lesion located on the negative side of the decision line), and PLP = per lesion positive (BCC measurements that have a corresponding lesion measurement on the positive side of the decision line).

contrast with a “per measurement” approach that would treat each measurement as an individual sample. In the “per measurement” analysis approach, a conflicting lesion classification could occur in instances when measurements from the same lesion are classified both positive and negative (i.e., lie on both sides of the decision line). One solution is a conservative diagnostic classification called “per lesion” analysis, as mentioned in our previous study.³⁴ Per lesion analysis classifies a lesion as positive if any one of the lesion’s measurements is classified as positive. Conversely, all of the lesion’s measurements have to be classified as negative in order for the lesion to be considered as negative. The basis of this classification was the dermatologist’s approach to err on the side of caution. To prevent training bias, classifier training was also performed per lesion.

Figure 7 illustrates the impact of a per measurement (a) versus a per lesion (b) analysis approach. For this example, we plot the two diagnostic PCs (D1 and D2) used to classify BCC from normal skin. In Fig. 7(a), there is one normal skin measurement on the positive (left) side of the decision line, and seven BCC measurements on the negative (right) side of the decision line. Using per measurement analysis, the sensitivity/specificity using this decision line is 82%/97% (32 of 39 BCC measurements and 37 of 38 normal skin measurements are correctly classified). However, five of these seven measurements incorrectly classified as normal measurements are from lesions with another measurement on the positive side of the decision line. While all measurements from lesion “1” are on the negative side of the decision line, measurements from normal skin “2” and lesion “3” both have a corresponding measurement on the positive side of the decision line. In Fig. 7(b), using per lesion analysis, lesion “1” is a per lesion false negative (PLFN) as all of its measurements are on the negative (right)

side of the decision line. Both normal skin “2” and lesion “3” would be classified as positive, because at least one of its measurements is on the positive side of the decision plane. As a result, normal skin “2” is a per lesion false positive (PLFP), while lesion “3” is per lesion positive (PLP), as shown in Fig. 7(b). The other BCC measurements on the negative side of the decision line have a measurement from the same lesion classified as positive (on the positive side of the decision line). Per lesion analysis gives a sensitivity and specificity of 95%/95% (18 of 19 BCC lesions and 18 of 19 normal skin measurements are correctly classified).

Acknowledgments

We appreciate the help, hospitality, and cooperation from all the staff, nurses, and physician assistants from MD Anderson’s Melanoma and Skin Care Center and Mohs and Dermatology Unit. We would like to thank all the doctors who have agreed to participate in this study: Dr. Janice Cormier, Dr. Valencia Thomas, and Dr. Deborah MacFarlane. We are also indebted to the patients who agreed to participate in this study. This work was supported by the Coulter Foundation, NIH R21 EB015892, CPRIT RP130702, and DermDX. Tunnell is listed as an inventor on an IP that is owned by University of Texas and licensed by DermDX.

References

1. H. W. Rogers et al., “Incidence estimate of nonmelanoma skin cancer in the United States, 2006,” *Arch. Dermatol.* **146**(3), 283–287 (2010).
2. R. Siegel et al., “Cancer statistics, 2011: the impact of eliminating socioeconomic and racial disparities on premature cancer deaths,” *CA: Cancer J. Clin.* **61**(4), 212–236 (2011).

3. N. Howlader et al., (Eds.), *SEER Cancer Statistics Review, 1975–2008*, National Cancer Institute, Bethesda, Maryland (2011).
4. G. Moreno et al., "Prospective study to assess general practitioners' dermatological diagnostic skills in a referral setting," *Australas. J. Dermatol.* **48**(2), 77–82 (2007).
5. H. Tran et al., "Assessing diagnostic skill in dermatology: a comparison between general practitioners and dermatologists," *Australas. J. Dermatol.* **46**(4), 230–234 (2005).
6. B. A. Shoo, R. W. Sagebiel, and M. Kashani-Sabet, "Discordance in the histopathologic diagnosis of melanoma at a melanoma referral center," *J. Am. Acad. Dermatol.* **62**(5), 751–756 (2010).
7. V.-D. Tuan and C. Brian, "Fluorescence spectroscopy for biomedical diagnostics," in *Biomedical Photonics Handbook*, V.-D. Tuan, Ed., CRC Press (2003).
8. B. G. Frushour and J. L. Koenig, "Raman-scattering of collagen, gelatin, and elastin," *Biopolymers* **14**(2), 379–391 (1975).
9. K. Sokolov, M. Follen, and R. Richards-Kortum, "Optical spectroscopy for detection of neoplasia," *Curr. Opin. Chem. Biol.* **6**(5), 651–658 (2002).
10. L. Perelman et al., "Observation of periodic fine structure in reflectance from biological tissue: a new technique for measuring nuclear size distribution," *Phys. Rev. Lett.* **80**(3), 627 (1998).
11. J. R. Mourant et al., "Light scattering from cells: the contribution of the nucleus and the effects of proliferative status," *J. Biomed. Opt.* **5**(2), 131–137 (2000).
12. M. Yelderman and W. J. New, "Evaluation of pulse oximetry," *Anesthesiology* **59**(4), 349–351 (1983).
13. B. J. Tromberg et al., "Non-invasive *in vivo* characterization of breast tumors using photon migration spectroscopy," *Neoplasia* **2**(1), 26–40 (2000).
14. F. Koenig et al., "Spectroscopic measurement of diffuse reflectance for enhanced detection of bladder carcinoma," *Urology* **51**(2), 342–345 (1998).
15. J. R. Mourant et al., "Spectroscopic diagnosis of bladder cancer with elastic light scattering," *Lasers Surg. Med.* **17**(4), 350–357 (1995).
16. I. J. Bigio et al., "Diagnosis of breast cancer using elastic-scattering spectroscopy: preliminary clinical results," *J. Biomed. Opt.* **5**(2), 221–228 (2000).
17. Z. Volynskaya et al., "Diagnosing breast cancer using diffuse reflectance spectroscopy and intrinsic fluorescence spectroscopy," *J. Biomed. Opt.* **13**(2), 024012 (2008).
18. M. Rahman et al., "Low-cost, multimodal, portable screening system for early detection of oral cancer," *J. Biomed. Opt.* **13**(3), 030502 (2008).
19. R. Drezek et al., "Understanding the contributions of NADH and collagen to cervical tissue fluorescence spectra: modeling, measurements, and implications," *J. Biomed. Opt.* **6**(4), 385–396 (2001).
20. H. P. Buschman et al., "Raman microspectroscopy of human coronary atherosclerosis: biochemical assessment of cellular and extracellular morphologic structures *in situ*," *Cardiovasc. Pathol.* **10**(2), 69–82 (2001).
21. H. P. Buschman et al., "Diagnosis of human coronary atherosclerosis by morphology-based Raman spectroscopy," *Cardiovasc. Pathol.* **10**(2), 59–68 (2001).
22. I. Georgakoudi et al., "Fluorescence, reflectance, and light-scattering spectroscopy for evaluating dysplasia in patients with Barrett's esophagus," *Gastroenterology* **120**(7), 1620–1629 (2001).
23. S. Sigurdsson et al., "Detection of skin cancer by classification of Raman spectra," *IEEE Trans. Biomed. Eng.* **51**(10), 1784–1793 (2004).
24. A. Garcia-Urbe et al., "Skin cancer detection by spectroscopic oblique-incidence reflectometry: classification and physiological origins," *Appl. Opt.* **43**(13), 2643–2650 (2004).
25. J. K. Patel et al., "Newer technologies/techniques and tools in the diagnosis of melanoma," *Eur. J. Dermatol.* **18**(6), 617–631 (2008).
26. M. Elbaum et al., "Automatic differentiation of melanoma from melanocytic nevi with multispectral digital dermoscopy: a feasibility study," *J. Am. Acad. Dermatol.* **44**(2), 207–218 (2001).
27. D. Gutkowitz-Krusin et al., "Precision of automatic measurements of pigmented skin lesion parameters with a Melafind (TM) multispectral digital dermoscope," *Melanoma Res.* **10**(6), 563–570 (2000).
28. M. Michalska, G. Chodorowska, and D. Krasowska, "SIAscopy—a new non-invasive technique of melanoma diagnosis," *Annales Universitatis Mariae Curie-Skłodowska. Sectio D: Medicina* **59**(2), 421–431 (2004).
29. J. H. Zhao et al., "Real-time raman spectroscopy for noninvasive skin cancer detection—preliminary results," in *2008 30th Annual Int. Conf. IEEE Engineering in Medicine and Biology Society*, Vols. 1–8, pp. 3107–3109, IEEE, New York (2008).
30. A. Garcia-Urbe et al., "In vivo diagnosis of melanoma and nonmelanoma skin cancer using oblique incidence diffuse reflectance spectrometry," *Cancer Res.* **72**(11), 2738–2745 (2012).
31. M. Judith and B. Irving, "Elastic-scattering spectroscopy and diffuse reflectance," in *Biomedical Photonics Handbook*, CRC Press (2003).
32. P. A. Jones and Y. A. DeClerck, "Destruction of extracellular matrices containing glycoproteins, elastin, and collagen by metastatic human tumor cells," *Cancer Res.* **40**(9), 3222–3227 (1980).
33. A. S. Haka et al., "Diagnosing breast cancer by using Raman spectroscopy," *Proc. Natl. Acad. Sci. U. S. A.* **102**(35), 12371–12376 (2005).
34. N. Rajaram et al., "Pilot clinical study for quantitative spectral diagnosis of non-melanoma skin cancer," *Lasers Surg. Med.* **42**(10), 716–727 (2010).
35. J. T. Motz et al., "Real-time Raman system for *in vivo* disease diagnosis," *J. Biomed. Opt.* **10**(3), 031113 (2005).
36. J. T. Motz et al., "Optical fiber probe for biomedical Raman spectroscopy," *Appl. Opt.* **43**(3), 542–554 (2004).
37. N. Rajaram et al., "Design and validation of a clinical instrument for spectral diagnosis of cutaneous malignancy," *Appl. Opt.* **49**(2), 142–152 (2010).
38. C. A. Lieber and A. Mahadevan-Jansen, "Automated method for subtraction of fluorescence from biological Raman spectra," *Appl. Spectrosc.* **57**(11), 1363–1367 (2003).
39. A. D. Meade et al., "Growth substrate induced functional changes elucidated by FTIR and Raman spectroscopy in *in-vitro* cultured human keratinocytes," *Anal. Bioanal. Chem.* **387**(5), 1717–1728 (2007).
40. S.-C. Dimitra et al., "Spectroscopic data of biologically and medically relevant species and samples," in *Biomedical Photonics Handbook*, CRC Press (2003).
41. C. A. Lieber et al., "Raman microspectroscopy for skin cancer detection *in vitro*," *J. Biomed. Opt.* **13**(2), 024013 (2008).
42. M. Gniatecka et al., "Melanoma diagnosis by Raman spectroscopy and neural networks: Structure alterations in proteins and lipids in intact cancer tissue," *J. Invest. Dermatol.* **122**(2), 443–449 (2004).
43. Z. W. Huang et al., "Raman spectroscopy of *in vivo* cutaneous melanin," *J. Biomed. Opt.* **9**(6), 1198–1205 (2004).
44. L. McArdle et al., "Protein tyrosine phosphatase genes downregulated in melanoma," *J. Invest. Dermatol.* **117**(5), 1255–1260 (2001).
45. Y. Xie et al., "The Raman detection of peptide tyrosine phosphorylation," *Anal. Biochem.* **332**(1), 116–121 (2004).
46. M. C. Skala et al., "Comparison of a physical model and principal component analysis for the diagnosis of epithelial neoplasias *in vivo* using diffuse reflectance spectroscopy," *Opt. Express* **15**(12), 7863–7875 (2007).
47. D. Weedon, "Tumors of the Epidermis," in *Skin Pathology*, 2nd ed., pp. 753–802, Churchill Livingstone, London (2002).
48. S. Edge et al., Eds., "Tumors of the epidermis," in *AJCC Cancer Staging Manual*, 7th ed., pp. 301–314, Springer, New York (2010).
49. E. Salomatina et al., "Optical properties of normal and cancerous human skin in the visible and near-infrared spectral range," *J. Biomed. Opt.* **11**(6), 064026 (2006).
50. S. M. Dinehart et al., "Metastatic cutaneous squamous cell carcinoma derived from actinic keratosis," *Cancer* **79**(5), 920–923 (1997).
51. N. Rajaram, T. H. Nguyen, and J. W. Tunnell, "Lookup table-based inverse model for determining optical properties of turbid media," *J. Biomed. Opt.* **13**(5), 050501 (2008).
52. M. Panjehpour et al., "Laser-induced fluorescence spectroscopy for *in vivo* diagnosis of non-melanoma skin cancers," *Lasers Surg. Med.* **31**(5), 367–373 (2002).
53. Q. G. Zhang et al., "Turbidity-free fluorescence spectroscopy of biological tissue," *Opt. Lett.* **25**(19), 1451–1453 (2000).
54. M. Sharma et al., "A novel multimodal fiber-optic probe and spectroscopy system for the early detection of skin cancer," *Rev. Sci. Instrum.* **85**(8), 083101 (2014).
55. H. Lui et al., "Real-time Raman spectroscopy for *in vivo* skin cancer diagnosis," *Cancer Res.* **72**(10), 2491–2500 (2012).
56. M. Gniatecka et al., "Diagnosis of basal cell carcinoma by Raman spectroscopy," *J. Raman Spectrosc.* **28**(2–3), 125–129 (1997).

57. A. Nijssen et al., "Discriminating basal cell carcinoma from perilesional skin using high wave-number Raman spectroscopy," *J. Biomed. Opt.* **12**(3), 034004 (2007).
58. K. E. Shafer-Peltier et al., "Model-based biological Raman spectral imaging," *J. Cell. Biochem.* **87**(8), 125–137 (2002).
59. K. E. Shafer-Peltier et al., "Raman microspectroscopic model of human breast tissue: implications for breast cancer diagnosis *in vivo*," *J. Raman Spectrosc.* **33**(7), 552–563 (2002).

Liang Lim is a postdoctoral fellow at the Princess Margaret Cancer Centre/University Health Network. He received his BS degree in electrical engineering and his PhD degree in biomedical engineering from the University of Texas at Austin, in 2004 and 2013, respectively. His current research interests include spectroscopy, SERS, and photoacoustic imaging. He is a member of SPIE.

Biographies of the other authors are not available.